Material transfer and subduction channel segmentation at erosive continental margins: Insights from scaled analogue experiments

Article *in* Tectonophysics · October 2018

DOI: 10.1016/j.tecto.2018.10.019

CITATIONS
0

READS
191

4 authors, including:

Francisca Albert
Temuco Catholic University
2 PUBLICATIONS **0** CITATIONS
SEE PROFILE

Nina Kukowski
Friedrich Schiller University Jena
189 PUBLICATIONS **2,932** CITATIONS
SEE PROFILE

Tectonophysics 749 (2018) 46–61

Contents lists available at ScienceDirect

Tectonophysics

journal homepage: www.elsevier.com/locate/tecto

Material transfer and subduction channel segmentation at erosive continental margins: Insights from scaled analogue experiments

Francisca Albert[a,*], Nina Kukowski[b], Andrés Tassara[c,d], Onno Oncken[e]

[a] Universidad Católica de Temuco, Chile
[b] Friedrich-Schiller University Jena, Germany
[c] Universidad de Concepción, Chile
[d] Millenium Nucleus the Seismic Cycle along Subduction Zones, Minecom-ICM, Chile
[e] GFZ German Research Centre for Geosciences, Germany

ARTICLE INFO

Keywords:
Subduction erosion
Subduction channel
Analogue experiments

ABSTRACT

Whereas tectonically erosive convergent margins make up nearly 60% of all present-day convergent margins, processes and amounts of material transfer and recycling remain enigmatic. Removal of material from the frontal forearc leaves no features which could be imaged seismically or probed through drilling. Only a few scaled laboratory analogue experiments have analyzed material transfer at convergent margins characterized by long-term subduction erosion and none has focused on processes and amounts of material transfer and recycling.

Therefore, in this study, we attempt to identify potentially relevant parameters controlling material transfer in brittle, tectonically erosive forearcs. This is addressed by a series of sandbox experiments performed with granular materials. We here mainly focus on the amount of sediment that can be transported downdip through the subduction channel (SC).

We analyzed our experiments with regard to the evolution of internal and basal material transfer, material transfer mode patterns, wedge geometry and SC evolution. To achieve a truly erosive scenario, we built a large initial wedge representing the brittle forearc, featuring a moderately high-friction basal detachment, and composed of "strong" granular material. There was no incoming material. The slope of the wedge initially had a critical taper. Through opening a subduction gap (SG), the wedge was subject to rear material loss.

Our observations point to a close interaction between SC segmentation and wedge deformation. Basal erosion mainly took place beneath the middle-upper slope. Our experiments confirmed the strong influence of the SC on the wedge evolution. A larger amount of material loss led to the development of a SC with an inhomogeneous distribution of velocities along the base of the wedge, segmenting the SC and slope geometry. The latter was comparable to observations in natural forearcs, which are segmented into lower, middle and upper slopes.

1. Introduction

Currently, about 60% of global convergent margins are thought to be shaped by subduction erosion (e.g. von Huene and Scholl, 1991; Clift and Vannucchi, 2004; von Huene et al., 2004; Vannucchi et al., 2008; Stern, 2011). Structurally, such convergent margins are characterized by the absence of an accretionary wedge (von Huene and Scholl, 1991), by the frequent presence of a small frontal prism consisting of sediments or slumped material, and by a margin wedge consisting of upper plate igneous rock (Ranero and von Huene, 2000). The landward displacement of the trench (here defined as trench retreat), inland migration of the volcanic front, forearc subsidence, thinning, and truncation, as well as extensional structures identified across the sediment apron, and seaward tilting of the slope surface are features typical of erosive convergent margins (Fig. 1; Miller, 1970; Rutland, 1971, Scholl et al., 1980; von Huene and Lallemand, 1990). Subduction erosion is also typically associated to an erosional unconformity at the top of the igneous basement which is initially covered by continental to coastal deposits that rapidly grade into deep sea deposits indicating unusually high subsidence rates (von Huene and Scholl, 1991). This is one of the few diagnostic features left in these margins, which allows to identify former subduction erosion (e.g. Oncken, 1998). Material may be removed by frontal subduction from the tip of the margin or through basal erosion from the underside of the upper plate (Ranero and von

* Corresponding author.
E-mail addresses: francisca.albert@gmail.com, falbert@uct.cl (F. Albert), nina.kukowski@uni-jena.de (N. Kukowski), andrestassara@udec.cl (A. Tassara), onno.oncken@gfz-potsdam.de (O. Oncken).

https://doi.org/10.1016/j.tecto.2018.10.019
Received 17 May 2018; Received in revised form 7 October 2018; Accepted 14 October 2018
Available online 19 October 2018
0040-1951/

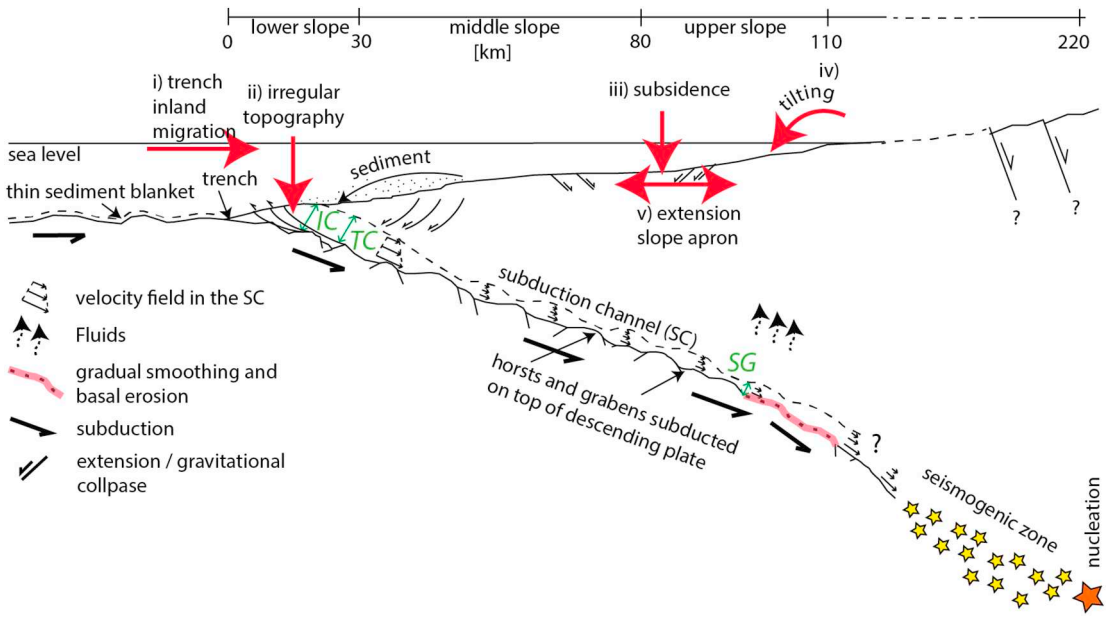

Fig. 1. Sketch illustrating the characteristics of an erosional convergent margin, based on conceptual models and seismic data (Cloos and Shreve, 1988a and b; von Huene and Ranero, 2003; Sage et al., 2006; Ranero et al., 2008). Typical features include a steeper slope than in accretionary systems, subsidence on the middle and upper slopes, gravitational collapse on the lower slope and a thin layer of sediment on the subducted plate. In general, the steepest segment corresponds to the lower slope, decreasing updip, where the shallowest segment corresponds to the upper slope. Lengths of the segments of the slope based on a Chilean profile example; small variations of these values are found along different margins. The vertical and horizontal variation in the velocity gradient of the basal flow corresponds to that observed in our experiments. The two control points IC and SG are the inlet and global capacities, as defined by Cloos and Shreve (1988a) in their SC model. IC is the theoretical inlet capacity, while TC is the measured thickness of the SC in our experiments (details in the text); SG is the equivalent to GC (Cloos and Shreve, 1988a). i–v are related to frontal and basal erosional processes (further details in the text). In the vicinity of the stick-slip zone, the horsts structures, cut by faults seem to be very deformed and begin to disintegrate landward, smoothing the surface of the lower plate (Tsuru et al., 2000). Basal erosion occurs below the middle-upper slope (Ranero and von Huene, 2000; von Huene and Ranero, 2003).

Huene, 2000).

It is estimated that ~83% of the incoming sediment is subducted at convergent margins, therefore plate convergence would favor material consumption instead of accumulation (Clift and Vannucchi, 2004). Whereas the geological record left at accretionary margins can be studied in situ, the record at erosive margins is limited due to the features mentioned above. The processes of consumption and further subduction of the eroded forearc material make investigating subduction erosion processes particularly difficult (von Huene and Scholl, 1991; Lallemand et al., 1992a; Oncken, 1998; Clift et al., 2003; Heki, 2004; Ranero et al., 2008), which is one of the main reasons why erosive margins remain enigmatic.

Erosive convergent margins are characterized by a trench without any sediment fill or sediments of just a few hundreds of meters thickness (e.g. von Huene et al., 1994; Ranero and von Huene, 2000; von Huene and Ranero, 2003; Calahorrano et al., 2008; Collot et al., 2011). Thus, any removal of material from the upper plate will lead to a net loss. Rates of subduction erosion can be estimated from such segments of convergent margins, the geometry of which is well known from wide angle seismic profiles and from subsidence information available from deep drilling (Vannucchi et al., 2004), assuming that the geometry has not changed through time. Estimates of long-term (> 10 Ma) subduction erosion along the Middle and South America margins are grossly in the order of 10 to 40 km^2/Ma (e.g. Vannucchi et al., 2004; Clift and Vannucchi, 2004; Kukowski and Onken, 2006; Stern, 2011). There are similar rates estimated from other erosive convergent margins like northern Japan (31–55 km^2/Ma in the last 20 Ma, von Huene and Lallemand, 1990) or South Sandwich (17.1 km^2/Ma in the last 15 Ma, Vanneste and Larter, 2002).

There is evidence that basal erosion can be two to four times more effective than frontal erosion (von Huene and Lallemand, 1990; Vanneste and Larter, 2002). It has also been suggested that material removed from the frontal forearc may be underthrusted and basally accreted at a more arcward location (e.g. Cloos and Shreve, 1988b; von Huene and Scholl, 1991; Lallemand et al., 1994). Whereas frontal subduction erosion may be facilitated by extensional failure of the tip of an erosive convergent margin, basal erosion may occur through removal of small amounts of material from the underside of the upper plate at certain periods during the earthquake cycle (Wang et al., 2010). However, the processes of material transfer across an erosive convergent margin remain only poorly understood so far.

Seismic reflection profiles (e.g. Calahorrano et al., 2008; Collot et al., 2011) and tomographic inversion using aftershocks from the Mw 8.0 Antofagasta earthquake in 1995 (Patzig et al., 2002) have revealed a thin zone of relatively low P wave velocities (approximately 0.5 to 3 km thick) almost parallel to the top of the subducting plate, which is interpreted as the subduction channel (SC), through which material is transported from a frontal position to greater depth. This subduction channel between the subducting and overriding plates and its important role for arcward material removal, was first recognized by Shreve and Cloos (1986). Parameters such as volume supply and density of sediment, subduction speed, and pressure gradient along the subduction channel (Shreve and Cloos, 1986) seem to govern SC behavior.

Laboratory analogue sandbox experiments, building on the critical taper concept (Davis et al., 1983), and employing sand and other granular materials like glass beads, sugar, or garnet sand, all representing sedimentary and igneous forearc rocks, have significantly helped to achieve our present understanding of material transfer at convergent margins (e.g. Gutscher et al., 1998a,b; Kukowski et al., 2002; Bonini, 2007; Nilforoushan et al., 2008; Graveleau et al., 2012 and references therein). Because the deformational behavior of granular materials reliably represents brittle rocks, such experiments can be used to quantify rates of material transfer, as long as boundary conditions are properly chosen and scaling is correct (Hubbert, 1937; Lallemand et al., 1992a; McClay, 1996; Schellart, 2000; Lohrmann

et al., 2003).

However, whereas there is an abundant wealth of experimental studies addressing the behavior of accretionary wedges (cf. Graveleau et al., 2012), only very few studies have addressed subduction erosion so far. Gutscher et al. (1998a) used an experimental set-up with an open subduction gate (global control point from Cloos and Shreve, 1988a) to force material removal through the SC. Basal erosion turned out as a parameter that crucially influences forearc basin formation from these experiments. A series of sandbox experiments addressing both accretionary and erosive convergent settings (Lohrmann et al., 2006) revealed that fluxes in the SC in both settings are temporally and spatially highly variable at short time scales (20 mm/yr at 100 mm/yr convergence). Numerical simulations confirm the switch to subduction erosion when no material is entering a subduction zone and infer that subduction erosion takes place in cases when there is at least a moderately strong interface zone (by either high frictional strength or shallow angle of subduction) between the subducting and overriding plates (Keppie et al., 2009).

Here, we present a series of 2D scaled erosional laboratory sandbox experiments to systematically explore structures and processes inherent to subduction erosion, such as material transfer and SC evolution, with a particular focus on the role of SG in forearc deformation. For this, we used brittle wedges representing the forearc. From the scaled physical models, we were able to identify characteristic patterns of material transfer by using particle image velocimetry (PIV) to visualize material flow. In particular, we focused on the effects of the amount of forearc material being transported downdip on the behavior of the SC and wedge mechanics by systematic variations of the size of the subduction gate.

2. Methodology

In our experiments, we simulated a purely erosional environment without any material entering the “trench” or “deformation front” (Lohrmann et al., 2006; Kukowski and Onken, 2006). This boundary condition ensures that the effect of subduction erosion on the forearc wedge is isolated from other processes which may influence its tectonic evolution. Our intention was to elucidate how the SG potentially controls modes, loci, and rates of frontal and basal erosion, as well as the kinematic evolution of an erosional wedge. We here focus on three experiments with a 2 mm, 4 mm and 6 mm thick subduction gate, to study how this parameter may affect forearc wedge evolution. With a scale factor of 105 (cf further below in this section), the thickness of the SC would be equivalent to about 200 m for G2, 400 m for G4 and 600 m for G6 in nature and therefore towards the lower end of the thickness of subduction channels observed at natural convergent margins (e.g. Lohrmann et al., 2006; Collot et al., 2011).

For our idealized model set-up, we built on previous analogue experimental studies where a “subduction window” had a significance in the resulting deformation, promoting tectonic erosion (e.g. Gutscher et al., 1998a; Lohrmann et al., 2003; Konstantinovskaja and Malavieille, 2005). The series of experiments we report here was carried out in a sandbox of 3 m length and 0.20 m width, with glass sidewalls (Fig. 2). A conveyor belt made of rubber to ensure a strong interface was placed on the rigid basal plate of the box and pulled by an engine with a constant velocity (~0.5 mm/s) representing the motion of a subducting oceanic plate. The basal angle β was zero for all experiments (we chose β = 0 after checking that having beta ≠ 0 yields similar results). A wedge-shaped body consisting of sieved sand and overlying the belt, represented a forearc wedge leaning against the vertical rigid backwall of the box (Fig. 2). The material composing the wedge was sifted in different layers separated by thin black sand layers to aid visual inspection. Additionally, triangular-shaped markers made of black sand were placed close to the glass panes to allow a better visualization of material paths (not influencing mechanical behavior; Lohrmann et al., 2003) and to identify internal deformation of the wedge.

We chose a mixture of sand and sugar as granular materials for the experiments, as these adequately represent the mechanical behavior of mechanically strong brittle forearc wedges (Hubbert, 1937; Lallemand et al., 1992b; Calassou et al., 1993; McClay, 1996; Lohrmann et al., 2003). The internal friction (μ) of the mixture is higher than that of sand ($\mu_{sand\text{-}sugar} = 0.598$ vs $\mu_{sand} = 0.541$; Table 1). We measured frictional properties of the used materials with a ring shear tester (Schulze, 2007). Since the base of the SC is equivalent to a continuously active internal shear zone at the base of the wedge, internal friction corresponds to the internal stable dynamic friction of the granular material (Table 1). As basal erosion occurs when basal strength is nearly equal to internal strength (i.e. $\mu_{basal} \approx \mu_{internal}$; Dahlen, 1984), the difference between the internal friction of the material and the basal friction along its contact with the conveyor belt was thus not larger than ~0.06 (the friction ratio $\mu_{BSD}/\mu_{SD} = 0.9$, Table 1) and an erosive regime was maintained (Gutscher et al., 1998b; Kukowski and Onken, 2006).

2.1.1. Scaling

For the system to develop dynamics similar to those observed in nature, mechanical properties of the analogue materials must be properly scaled. Cohesion (C) and density (ρ) of sedimentary or upper crustal rocks are C: 0.7–105 MPa and ρ: 2000–3000 kg m^{-3}, respectively (Landolt-Börnstein, vol. I “Physical properties of rocks” available at www.springerlink.com). Using the C and ρ values from analogue materials (Table 1) for the ratio $[C/\rho]_{nature}/[C/\rho]_{model}$, we finally obtained a scale factor of about 10^5 with up to about half an order of magnitude variation, which is in accordance with other analogue experimental studies (Hubbert, 1937; Lallemand et al., 1994; Koyi, 1997; Schellart, 2000; Kukowski et al., 1994; Gutscher et al., 1996).

All initial sand wedges built up through sieving the sand-sugar mixture had a constant slope of 13.5° and were 125 cm long. Boundary conditions of analogue experiments are often strict, like e.g. a solid back wall representing the static backstop (Kopp and Kukowski, 2003) in nature, which is why they may exert a dominant influence on experimental evolution. We therefore chose to build long initial wedges to make sure that at least the frontal 60 to 80 cm of the experimental wedges would show a behavior little influenced by the rear boundary condition. This would correspond to the frontal part of a natural forearc, which has been seismically imaged at high resolution at several subduction zones around the Pacific at least to a distance of 60 to 80 km arcward from the deformation front, where it can still have a thickness of more than a kilometer (e.g. Lohrmann et al., 2006; Collot et al., 2011). There are cases where subduction channels may extend to much larger depths and a position at least 150 km landward of the trench (Friederich et al., 2014). Thus, on the one hand we successfully avoid the boundary condition of the rear wall and subduction gap to influence processes close to the tip of the wedge and on the other hand, it is justified to assume that 120 km arcward of the deformation front, the subduction channel still has a significant thickness.

Experimental material transfer rates were specified as cm^2/cm_{conv} (i.e. cm^2 of material per cm of convergence) or cm/cm in case of one dimensional numbers (tip retreat and subsidence). In order to compare experimental results (in cm^2/cm_{conv}) with estimates of erosion rates from natural forearcs (in km^2/Ma), we used the 10 cm y^{-1} rate of convergence between the Nazca and South American plates (DeMets and Dixon, 1999) thus establishing a $10^2 \times [km^2/Ma]_{nature} = [cm^2/cm_{conv}]_{model}$ ratio. A total convergence of 500 cm like in all experiments reported here would cover a time span of 5 Ma in nature.

2.1.2. Monitoring experiments with the PIV system

Particle Imaging Velocimetry (PIV) is an optical, non-intrusive method originally developed for flow visualization of particles (White et al., 2001; Hampel et al., 2004). It allows monitoring displacement

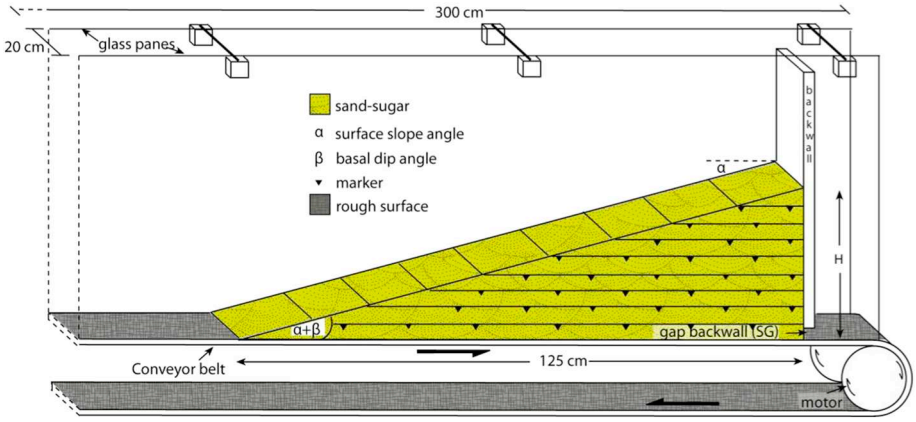

Fig. 2. Model configuration. The size of the gap at the bottom of the back-wall (SG) was specified for each experiment. Basal angle β is set to zero in all the experiments.

Table 1
Mechanical properties of used materials measured using a Ring Shear Tester, with a standard error smaller than 0.007 (RST-01, Schulze, 2007). μ_P: peak strength; μ_{SD}: stable dynamic strength; μ_{SS}: stable static strength; μ_{BSD}: coefficient of basal friction of the conveyor belt. C: cohesion.

Properties	Sugar	Mixture	Sand
		40% sand 60% sugar	
Grain size spectra [mm]	< 0.7	< 0.7	< 0.63
Filling method	Sifted	Sifted	Sifted
Bulk density [gr/cm^3]	0.97 (± 0.01)	1.40 (± 0.02)	1.71 (± 0.02)
C [Pa]	47(± 16)	< 40	< 40
μ_P	0.87 (± 0.006)	0.797 (± 0.004)	0.681 (± 0.004)
μ_{SS}	0.75 (± 0.002)	0.69 (± 0.001)	0.615 (± 0.002)
μ_{SD}	0.608 (± 0.003)	0.598 (± 0.001)	0.541 (± 0.001)
μ_{BSD} (conv. belt/material)		0.54 (± 0,001)	0.55 (± 0,002)
μ_{BSD}/μ_{SD}		0.9	1.02

from groups of particles between photographs taken with very short time intervals and a sufficiently high camera resolution. To do so, we used an 11 Mpx digital camera. Digital images using the PIV camera were taken every 4 s, equivalent to 2 mm of convergence (PIV accuracy of the displacement measurement could reach ~0.5 mm; Adam et al., 2005; further details in Albert, 2013), resulting in a total of ~2500 digital images per experiment.

3. Processes, material transfer, and measured quantities

Here, we explain how we identified segmentation in the wedges and how we estimated values for volumes of material transfer, in comparison with data from natural forearcs.

Horizontal and vertical components of the velocity field, v_x and v_y respectively, were derived from a base-parallel reference line above the conveyor belt. For v_x, the reference line is 4 mm above the conveyor belt (yellow in Fig. 3) and shows the velocity of the particles inside the SC. For v_y, the reference line is 10 mm above the conveyor belt (red in Fig. 3) and shows the vertical displacements of the particles inside the wedge close to the SC's upper shear zone (or shear zone upper boundary SZUB, section IV.3); upward and downward displacements of particles are indicated by positive and negative values, respectively.

Different material transfer modes (Frontal Erosion, Basal Accretion, and Basal Erosion) that took place during the experiments were identified by changes in the vertical position of the marker lines, and from the geometry of the wedge (Fig. 3). Basal accretion was identified by the upward motion of any marker line with respect to its previous horizontal position. Shortening of the wedge was quantified by measuring tip retreat. Basally eroded material was identified through the downward motion of a marker line, with respect to its previous horizontal position (Fig. 3).

To quantify the different material transfer modes, material transfer rates were determined from images every 50 cm of convergence. The change in position of the triangular markers and marker lines proved to be useful for the overall description and quantification of material transfer within the wedges. Thus, the area between two consecutive positions of the same marker line is used to estimate material transfer rates. For Basal Erosion, we used the 2nd marker line from the bottom of the wedge since the lowest one was consumed during the experimental run (Fig. 3). The rate of Frontal Erosion was calculated by the areal change of the leading edge of the frontal part of the wedge, from two consecutive images. The rate of subsidence was estimated from the areal change between the surface slope of the wedge from two consecutive images.

Estimated bulk rates for each material transfer mode were derived from quantities measured in the serial digital images corresponding to the cumulative values of material transfer rates divided by total convergence. With no external material supply (no incoming sand-layer), the only source for frontal underplating of material comes from frontal gravitational collapses.

Critical taper theory (Davis et al., 1983) suggests that a soil or sand wedge pushed by a bulldozer initially deforms internally until it achieves a critical shape, whereupon the wedge slides stably on its base. Quantitative analysis to compare the different mass transfer modes was carried out only after the first 50 cm of convergence, after termination of a transitional stage when the wedge and SC start showing a steadier behavior (Table 2).

There are two control points for fluxes and therefore for the capacity of a SC (Cloos and Shreve, 1988a,b): at the leading edge of the SC, the inlet capacity restricts the total amount of material going into the subduction channel (IC; Fig. 1) and the global control point is where the SC capacity decreases because of a sharp increase either in the density of the overlying rocks, of the forearc slope, or of the dip of the oceanic plate. The capacity of the SC at the global control point (global capacity or SG; Fig. 1) defines how much material will be subducted to greater depth. Both control points yield the IC/SG ratio as a parameter that may crucially influence SC behavior, and consequently forearc evolution. At the leading edge of the SC, both frontal erosion and accretion occurred simultaneously with the continuous retreat of the wedge toe. Thus, the determination of a precise location of the IC was problematic. As this resulted in poorly constrained data for IC, we estimated the fluxes at different points unaffected by boundary effects, called TC (Tip Capacity); TC was not determined exactly at the leading edge of the wedge,

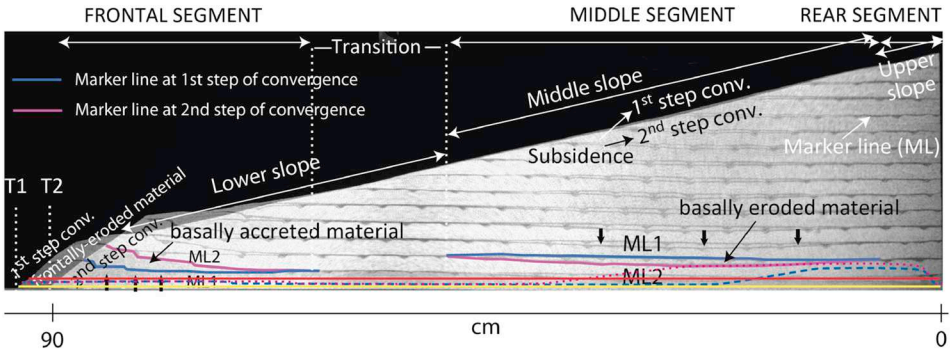

Fig. 3. The procedure to detect basal and frontal erosion, basal accretion and subsidence. The image shows two pictures from the experiment G6 superimposed at stages 100 cm and 150 cm of convergence. The wedge segmentation was defined by the loci of the different modes of mass transfer. T1, ML1 and T2, ML2 represent the position at first and second intervals of convergence, respectively of **T**ip and **M**arker **L**ine. Vertical arrows indicate the direction of the marker line movement, showing the positions of basal accretion and erosion. The areas between ML1 and ML2 account for rates of basal accretion (at front), and basal erosion (at middle segment). Basal erosion is observed at the surface as subsidence, defining a middle segment of the wedge and middle slope respectively. At the leading edge of the frontal segment, and at the middle slope segment, the missed area between the first and the second state (or step) accounts for the frontal eroded material and subsidence, respectively. Segmented and dashed lines represent the SZUB of the SC at 1st and 2nd step of convergence, respectively. (For interpretation of the references to colour in this figure, the reader is referred to the web version of this article.)

but slightly arcward (Fig. 1), where the thickness of the SC was well constrained. Fluxes at different points along the SC were estimated as the flow through a line perpendicular to the base of the wedge at specific distances from the backwall. We measured and compared the TC/SG ratios between the experiments, where the TC value represents the mean thickness of the Tip segment and SG the subduction gap size.

4. Results

As we use new concepts to analyze our experiments, here we carefully and extensively describe the evolution of our experiments with regard to the important segmentations we identified in our sand wedges, also include a cautious evaluation of our results, and thus are able to later transfer our results to nature.

4.1. Segmentation within the wedge

During convergence, all experimental wedges developed a particular segmentation, which corresponds to the location of various mass transfer modes (Fig. 3). At the Frontal part of the wedge, frontally eroded material was underthrusted and underplated. As a result, this area experienced shortening and uplifting. Basal material accretion mainly occurred in relation to activation of backthrusts. The Transition segment is located between the Frontal and the Middle segments and is associated with no vertical motion of the marker line. The Middle segment is where basal removal of material takes place. Thus, subsidence occurring in the middle slope is triggered by the removal of material from the base of the wedge (i.e. basal erosion). Finally, the most backward past of the wedge corresponds to the Rear segment. Slope geometry mirrored this segmentation.

Table 2
Rates and rate ranges during the second phase of the different mass transfer modes. The final thickness of the SC of the Tip, Central and Back segment was measured once they reached their final value and where they were thickest.

		Mass transfer modes	Rates cm^2/cm (highest/lowest)	Standard deviation	Mean value cm^2/cm	Final thickness mm
G6 experiment = 6 mm	2nd phase	Frontal erosion	20.6/7.6	5.21	13.7	
	(50–300)	Basal erosion	16.7/11.6	2.11	14.1	
		Basal accretion	11.8/1.6	4.22	4.8	
		Tip retreat	8.3/1	2.85	2.5	
		Tip-/Central-/Back-segment				~5/~4.6/~32
	(300–500)	Frontal erosion	17.5/10.5	2.67	13.1	
		Basal erosion	17.8/8.6	3.63	13.3	
		Basal accretion	7.7/0.0	2.95	3.9	
		Tip retreat	1.5/0.3	0.47	1.0	
		Tip-/Central-/Back-segment				~5/~4.6/~32
G4 experiment = 4 mm	2nd phase	Frontal erosion	42/17.3	8.00	28.2	
	(50–300)	Basal erosion	8.9/4.3	1.90	6.7	
		Basal accretion	32.5/8.7	8.82	22.3	
		Tip retreat	8.2/1.6	2.49	3.2	
		Tip-/Central-/Back-segment				~5.5/~5/~28
	(300–500)	Frontal erosion	41.7/2.0	14.76	21.4	
		Basal erosion	8.8/4.3	1.72	6.1	
		Basal accretion	32.5/19.3	5.85	24.6	
		Tip retreat	1.7/0.7	0.47	1.1	
		Tip-/Central-/Back-segment				~5.5/~5/~32
G2 experiment = 2 mm	2nd phase	Frontal erosion	32.1/14.5	6.61	24.0	
	(50–300)	Basal erosion	1.6/1.6	0	1.6	
		Basal accretion	29.2/3.5	9.83	15.9	
		Tip retreat	7.9/1	2.51	3.3	
		Tip-/Central-/Back-segment				~5.5/~5/~4
	(300–500)	Frontal erosion	27.0/14.1	5.83	20.4	
		Basal erosion	1.6/1.8	0.08	1.7	
		Basal accretion	29.2/14.7	5.77	21.8	
		Tip retreat	1.9/0.6	0.50	1.2	
		Tip-/Central-/Back-segment				~5.5/~5/~4

4.2. Kinematic evolution of erosional wedges

Two phases of kinematic evolution of the erosional wedges were identified for our experiments on the basis of material transfer as shown in Figs. 4i–vi and 5.

4.2.1. First phase

This phase, which covered the first 50 cm of convergence, is characterized by fast compaction of the material within the wedges and diffuse deformation in its frontal portion. During this phase, the wedges of experiments G4 and G6 can be subdivided into four segments: A short, Frontal segment, in which frontal erosion and basal accretion take place simultaneously. This segment underwent the largest changes in shape. It became narrower but steeper, and developed a bulge in the rear of which potential accumulation space was created.

The long Transition segment seems to be largely unaffected by material flux taking place within the subduction channel, whereas the Middle segment undergoes basal erosion (Figs. 3 and 4). The Rear segment is characterized by the development of the thickest subduction channel. At the beginning of the experiment, tip retreat was much faster than at any later moment (Fig. 5a). Thus, this phase marks the evolution of the wedge from its initial conditions and geometry to a wedge the geometry and segmentation of which is mainly controlled by the boundary conditions.

4.2.2. Second phase

This phase is characterized by a temporal fluctuation of the amounts and rates of erosion and accretion. Rates of material flux and the upward and downward displacements of particles during the first 250 cm of convergence are the largest compared to any other period during

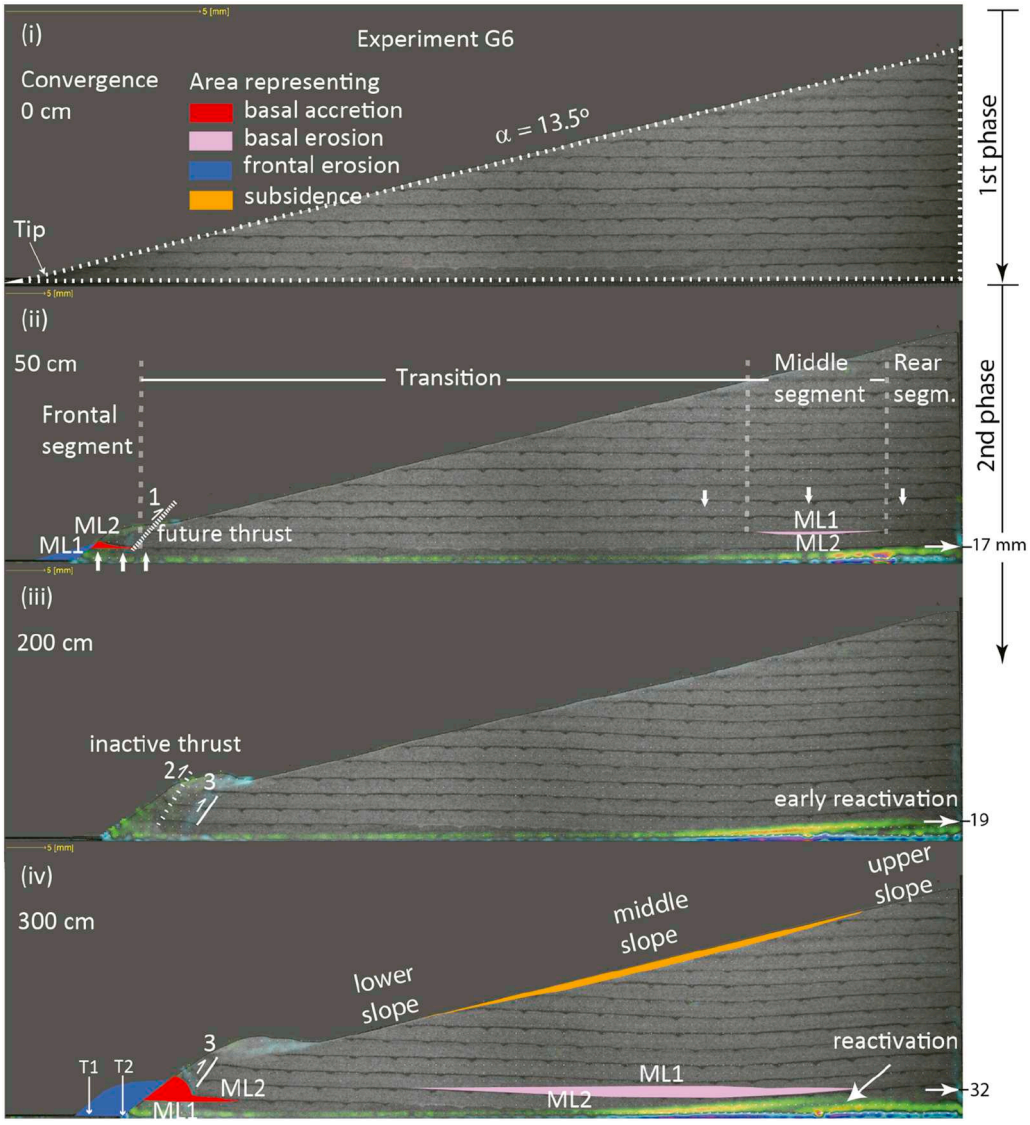

Fig. 4. i)–vi) Evolution of the experiment G6 through time. Horizontal white arrows show the maximum thickness (mm) of the SC at each interval. Numbers indicate successive initiation of backthrusts. Symbology is the same as in Fig. 3. i) Initial state. ii) Around 50 cm of convergence the first thrust occurred. iii) Around 200 cm of convergence an early reactivation of fault was recognized at the top of the basal shear zone (Back segment). iv) The reactivation of a fault and the current subdivision of the slope (lower, middle and upper) are shown. v) The white dashed rectangles are enlarged above and show part of the 1) Tip-, 2) Central- and 3) Back segment of the basal shear zone of the SC. A close-up of the SC shows the velocity vectors variations along it, and also the thickness at the inlet (IC) and at the rear (SG). Black arrows point out differences of velocity vectors throughout the SC. They illustrate the magnitude and direction of displacement of single particles inside the active shear zone. vi) Snapshot at the end of the process. The Transition zone became a single line, by the union of the Frontal and Middle segments. The initial geometry of the wedge was compared with the last state geometry (dashed lines). vii) Close-up of the SC from a digital image recorded by PIV during thrust reactivation from one of the experiments. A segmented flow behavior is observed, decreasing the final amount of transported material inside the SC.

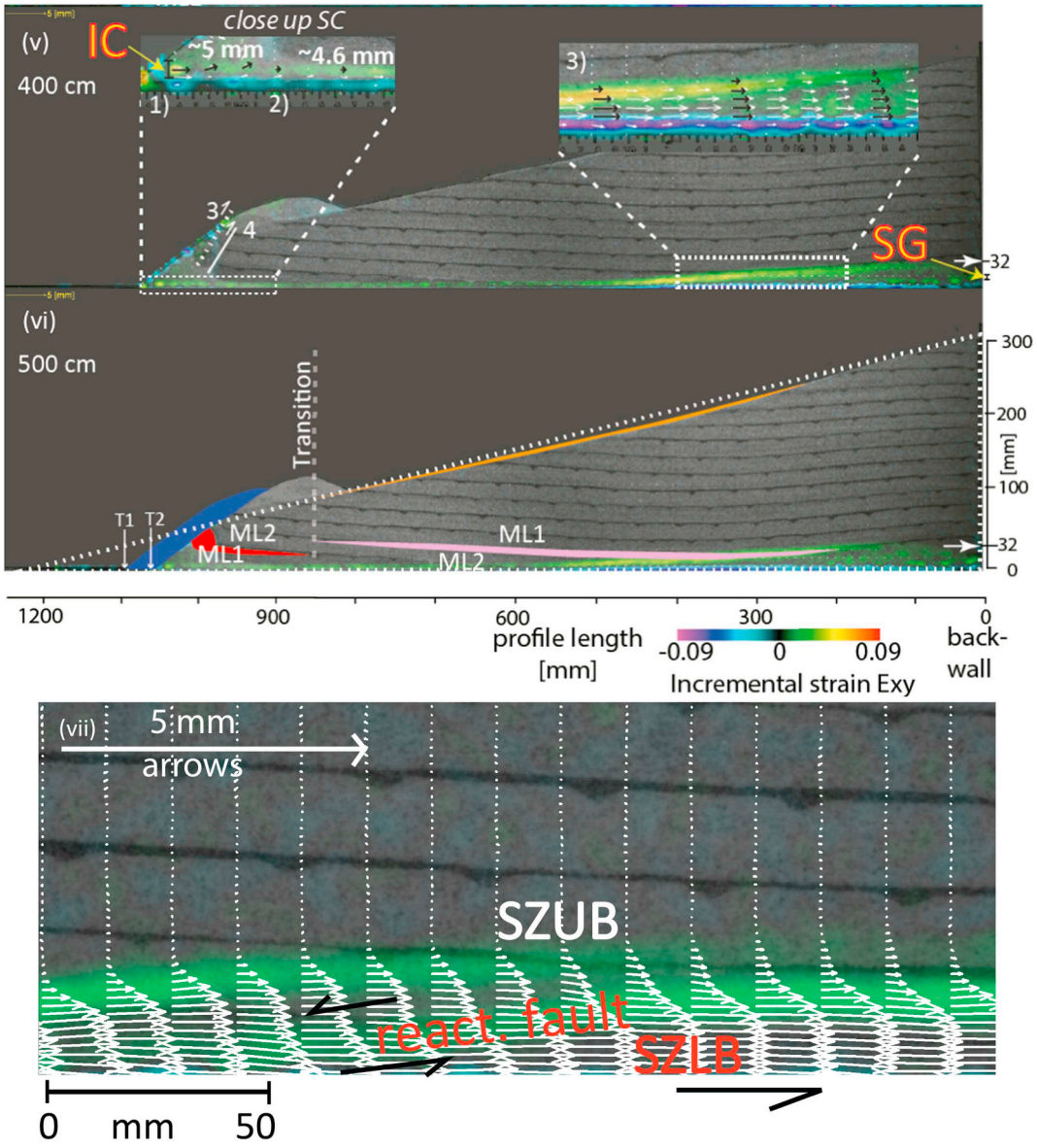

Fig. 4. (*continued*)

convergence (Figs. 5, 6b and 7a and b). Frontal and basal erosion in experiments G4 and G6 affect continuously larger parts of the wedge, indicating that the Frontal segment is growing, while at the same time its tip is further retreating, although much slower than initially (Figs. 4ii and iii, 5a, and 6a.i–iii and b.v–vii respectively). At the same time, rates of frontal erosion exceed those of basal accretion and basal erosion (Table 2; Fig. 5a). The volume of basally eroded material was almost zero in G2 and highest in experiment G6 (Table 2). Basal accretion rates were similar in G2 and G4, and in both experiments larger than in G6 (Table 2; Fig. 5a).

After 300 cm of convergence, material flux was more uniform than previously and transferred material volumes were slightly smaller than right before (Fig. 5, Table 2). In experiment G4, a forethrust in the rear part of the wedge affected material flux and thrusting at the Frontal segment of the wedge (Fig. 7b). Subsidence was highest in experiment G6 with the widest SG and reached almost null for G2 (the narrowest SG).

During this phase, the Middle segment is continuously becoming longer, implying that the Transition segment is becoming shorter. Closely above the area affected by basal erosion, subsidence of the wedge occurred, leading to the formation of a mid-slope basin (Fig. 4iv). The size of the Transition segment was further decreasing, whereas the area affected by basal erosion, the Middle segment, grew towards the tip of the wedge (Fig. 6b.vii, .viii). Finally, the Transition segment almost disappeared (Fig. 4vi). Fault reactivation in the G6's Rear segment took place at around 260 cm of convergence (Fig. 4iii, iv and vii).

4.3. Segmentation and kinematics of the subduction channel

An important feature of our models was the evolution of a SC, which was bounded by active upper (SZUB) and lower (SZLB) shear zones, respectively (Fig. 8). SZLB kinematics was controlled by the stable dynamic internal friction; SZUB kinematics was controlled by the three values of internal friction in different periods over time (Table 1). The vertical position of the SZUB determined three different thicknesses of the SC. The “Tip segment” begins at the toe and continues to the point where the shear *décollement* steps down. Rearwards, the “Central segment” ends with the thickening of the SC, which is characteristic for the “Back segment” which continues to the backwall. In experiment G6 at around 260 cm of convergence, fault reactivation started in the rear part of the Back segment (Fig. 4iii), afterwards migrated tipwards and

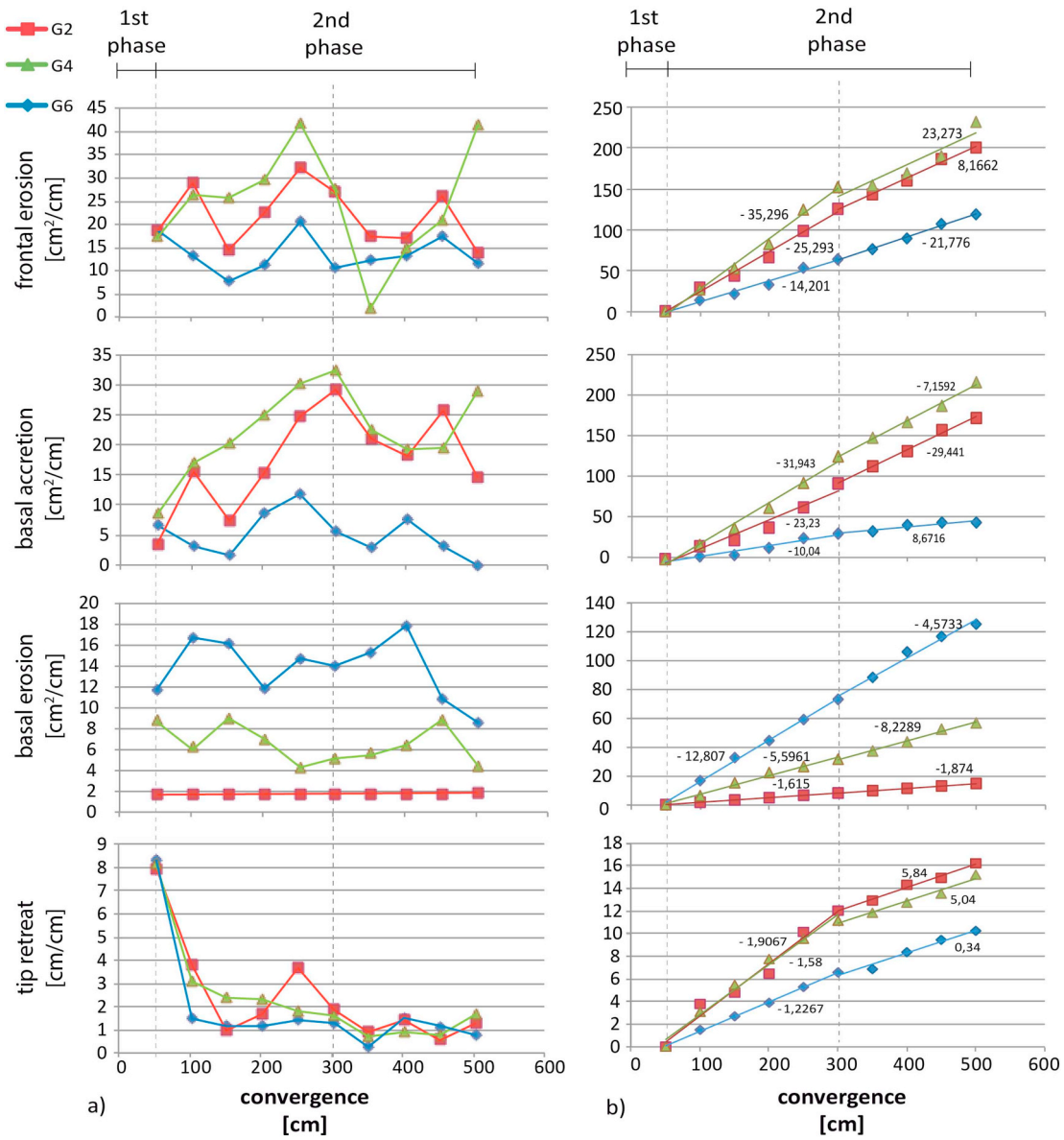

Fig. 5. a) Comparison of the different mass transfer rates of experiments of the first series SG while testing different subduction gaps, after the wedges deviated from the initial conditions. b) Comparison between the different mass transfer volumes of the series. Quantities were normalized for direct comparison of volumes (initial values are stated null at 50 cm of convergence). Note the slope variation after 300 cm of convergence of the trend line. Numbers next to the trend line indicate the value of the slope. cm/cm is cm of tip retreat per cm of convergence.

settled between 100 and 200 cm tipwards of the backwall (Figs. 4iv, vii and 9). Whenever a reactivation of that fault occurred, downward displacement of particles was locally activated by block rotation over the reactivated roof fault (c.f. Fig. 6a.iii and b.vii).

These segments were present during the entire experimental runs, but their length and thickness changed with time. In experiments G4 and G6, the Back segment became longer through the incorporation of "flowing" material and also became thicker (Figs. 4iii–iv, 7b, 8 and 9). Likewise, we observed inland migration of the inner edge of the Tip segment along with rearward displacement by backthusting (Figs. 3 and 8). All experiments reached their final SC thickness and overall geometry shortly before 3 m of convergence (Table 2; Figs. 4iv–vi and 9) implying that material fluxes achieved a quasi-dynamic steady state by then. The Central segment was marked by a relatively uniform strain (Fig. 8 Central1 and Central2) and as soon as the SC became thicker, strain rate increased (Fig. 8 Back1 and Back2).

Horizontal and vertical particle velocity variations are related to thickness changes of the SC and roughly coincide with the internal segmentation of the wedge (Figs. 6a.i–iii, 7a and b). The vertical velocity component decreased upwards from the SZLB (with the largest velocity $u = u_0$), reaching the SZUB at its lowest value $u \approx 0$ ($u_0 \sim$ velocity of the conveyor belt). Vertical upward or downward displacements of the particles were related to the largest absolute values of the vertical component of the velocity field (Fig. 6b). In experiments G4 and G6, we observed that the largest downward displacement of particles took place in two regions: in front of the fastest particles and at the rear, next to the backwall, respectively. Particle flux also varied inside the SC. Flux at the Tip segment was faster than along the Central segment for all experiments and the horizontal velocity component decreased from the tip rearwards (Fig. 8 Tip1 and Tip2). At the Back segment, flux was slow just before the second phase, accelerating afterwards (Fig. 6c). The Back segment showed faster velocities than the Central segment in experiments G6 and G4 (Figs. 6a, b and 7b), but only G6 had the fastest particles at the Back segment. In experiment G6 a decrease of flux was observed at about 300 cm of convergence (Fig. 6a.iii and c at 20 cm profile length), and afterwards, total flux

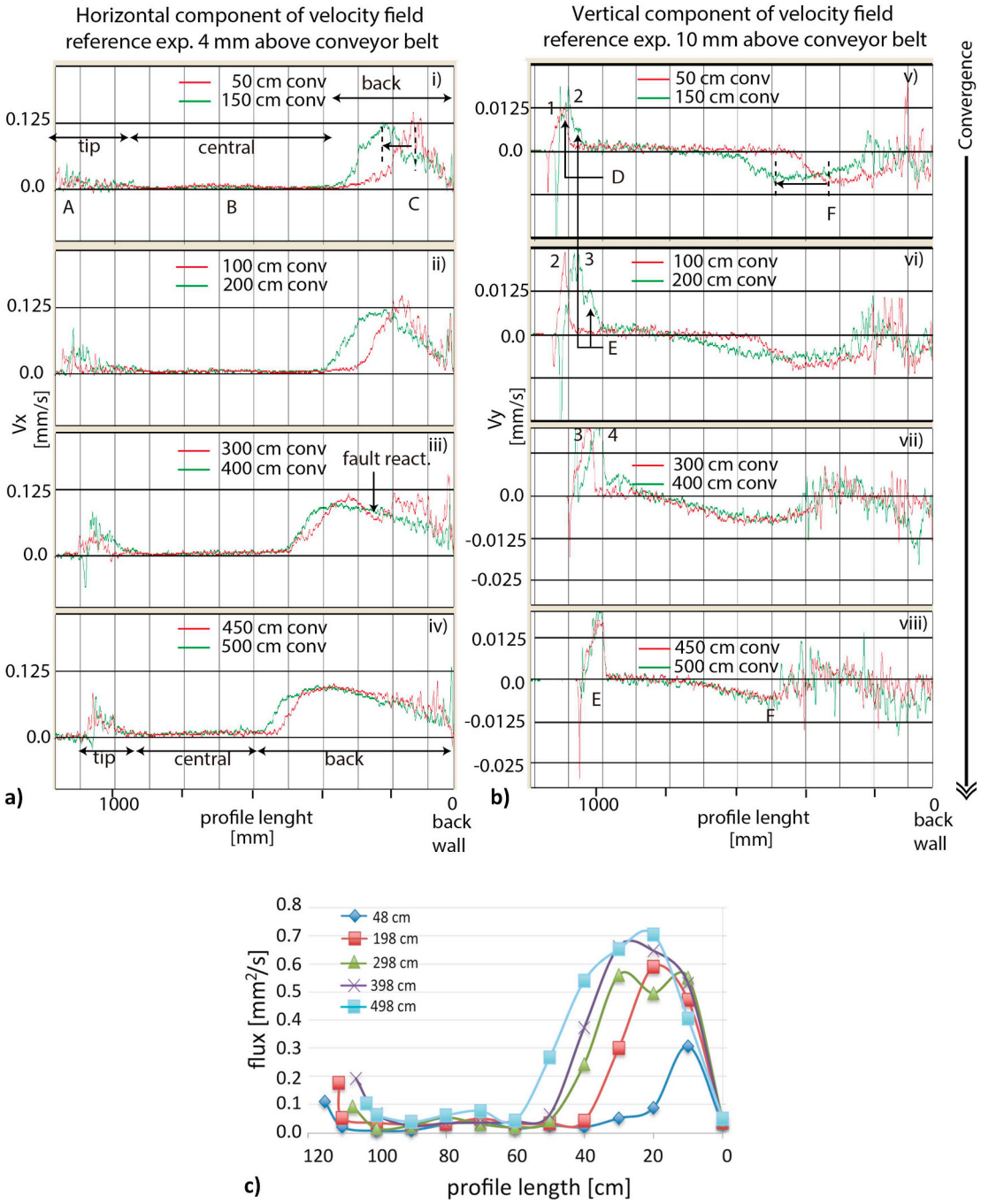

Fig. 6. a) Horizontal component of the velocity field and b) Vertical component of the velocity field, as derived from Fig. 3 (yellow line at 4 mm and red line and 10 mm above the conveyor belt, respectively), during different convergence intervals. Velocity (horizontal component of the velocity field) distribution defines SC segmentation into Tip, Central and Back (see also Fig. 8). From slowest to fastest, this order: B, A and C. Notice the forward migration of the fastest particles between one stage and the following. Characteristics of vector velocity field correlate with the vertical particle displacement (vertical component of the velocity field), providing a tool to localize specific mass flows as erosion or underplating. D denotes the upward movement of the particles by activation of thrusts and id numbers the active thrusts in Fig. 4. E denotes the upward displacement by underplating and F the downward displacement of the particles. The forward migration of F correlates with the migration in C. Velocities are instantaneous velocities. c) Fluxes of the SC at different stages of convergence. A decline of flux matches the thrust at the Back segment at 300 cm of convergence. (For interpretation of the references to colour in this figure legend, the reader is referred to the web version of this article.)

remained approximately the same (Fig. 6c).

Forward migration of subsidence was noticed along with forward migration of the fastest particles in the frontal part of the Back segment (Figs. 4i–vi, 6b and 7b). In experiment G2 overall particle velocity was quite uniform behind the Tip segment and therefore, a Back segment was not observed (Fig. 7a). Likewise, inland migration of the inner edge of the Tip segment correlated with rearward displacement of the Frontal segment (Figs. 4i–vi and 8). During the last 50 cm of convergence of G6 wedge evolution, the area affected by particles moving downward became smaller, which was mirrored by a drop of basal erosion rates (Fig. 6b.viii). Consequently, slower forward migration of the fastest particles in the Back segment and rearward migration of the Tip were also observed (cf. Fig. 6b.vii and .viii). Thus, along with a faster displacement of material, the Back segment in experiment G6

covered the largest area, compared to experiments G4 and G2 respectively.

4.4. Quantification of material transfer

We first computed incremental material transfer rates for each 50 cm of convergence to investigate if material flux is continuous or episodic. Our observations indicate that all accretionary and erosive material fluxes vary significantly within the second phase of the experiments without any defined trends (Fig. 5a), whereas cumulative fluxes showed almost linear trends, with fluxes and tip retreat mostly being somewhat slower after 300 cm of convergence (Fig. 5b; Table 2). We then computed bulk fluxes for each type of material transfer for an entire experiment and expressed the transferred volumes in units which would be adequate for natural forearcs for later comparison with nature (Fig. 10). Although we only varied one parameter in a systematic way, only basal erosion and subsidence mirrored this trend, whereas all other material fluxes were highest in experiment G4 with the SG being 4 mm thick. Only in experiment G6, basal erosion (52%) contributed more to subduction erosion than frontal erosion (48%), whereas in experiments G4 and G2, basal erosion accounted for 20%, and 6% of total erosion, respectively. Basal accretion occurred also in experiment G6 with the thickest SG, but its volume was only about 20% of that of total erosion.

In order to compare fluxes among the experiments, two strategic positions along the SC were chosen. One point, CC (Central Capacity), located at 60 cm from the backwall (Fig. 9) was never affected by either accretion or basal erosion throughout convergence. The second point, BC (Back Capacity), at 30 cm from the backwall (Fig. 9) was located where basal erosion occurred in order to determine the effect of SG size on the flux. In experiments G2 and G4, particle velocity and SC thickness were similar at the point CC, while G6 had the thickest SC with the slowest flux velocity. Thus, flux was similar in all experiments and increased over time (Table 3 and Fig. 11a). At the position BC, the forward migration of the Back segment started to impact on the SC's flux after 150 cm and 200 cm of convergence for experiments G4 and G6, respectively. Here, thickening of the SG led to an increase in material transfer volume (Table 3 and Fig. 11b). However, not only SC size controlled flux, but also internal shear zones within the SC. Fault reactivation at the Middle segment observed in experiment G6 along a well-developed shear zone defined two domains of horizontal displacement of particles inside the SC. Those particles, located between the boundaries of the reactivated fault, showed a horizontal component of the velocity field that increased from the top to its base (Fig. 4vii). The particles inside the areas below the shear zone were characterized by a uniform and faster horizontal displacement. As a result, total flux decreased because of this local deceleration. Therefore, the reactivation of faults at the Back segment was mirrored by a local decline of flux (Fig. 6c).

At the Tip segment, the accretion of basal material caused uplift and migration rearwards of the Frontal segment by episodic activation of

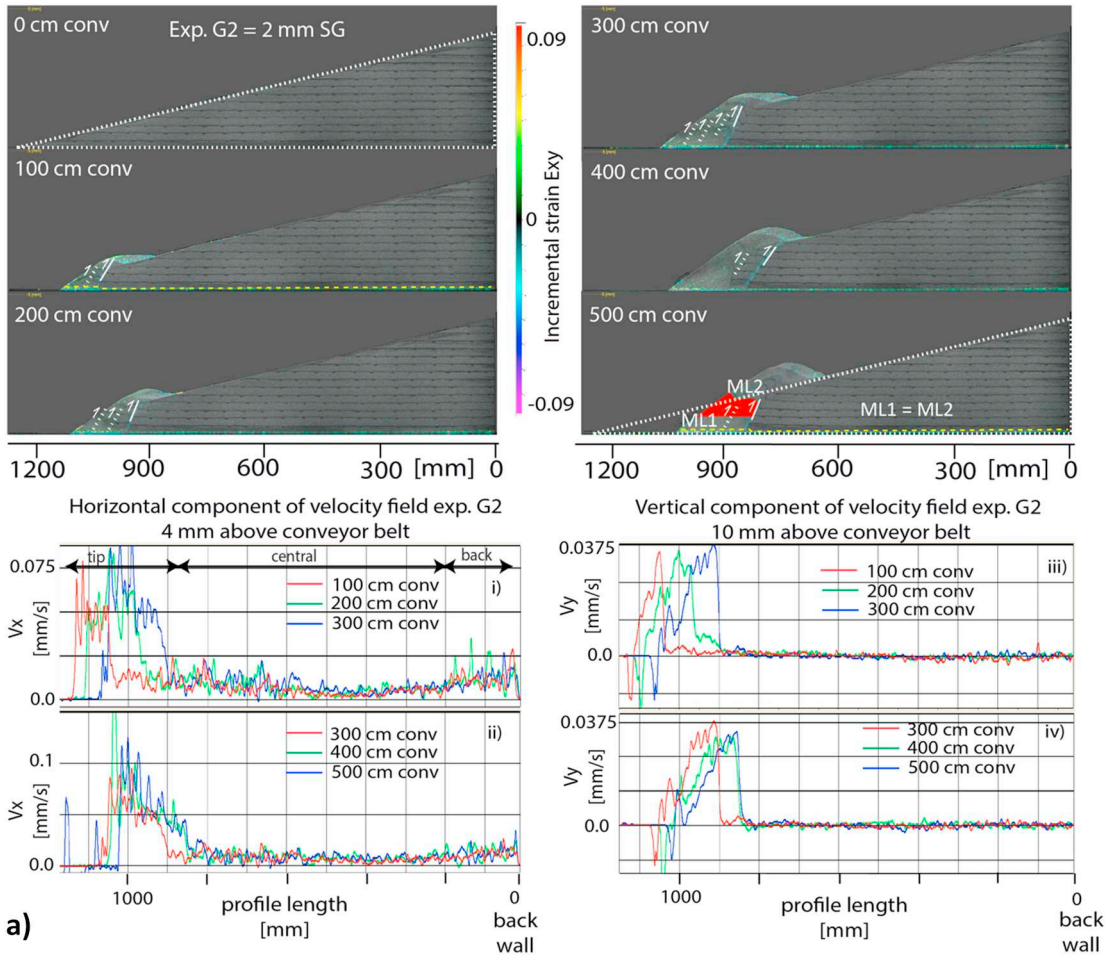

Fig. 7. Snapshots of experiments every 100 cm of convergence, for subduction gaps a) 2 mm and b) 4 mm, respectively. The corresponding particle horizontal velocity vx (measured at 4 mm above the conveyor belt) and vertical velocity vy (measured at 10 mm above the conveyor belt) are directly compared to each other. Initial geometry of the wedge is compared with the last state geometry (dashed lines). Yellow dashed line represents the SZUB of the SC at 100 and 500 cm of convergence. Symbology is the same as in Fig. 4. ML1 represents the position of the **M**arker **L**ine at 0 cm of convergence. (For interpretation of the references to colour in this figure legend, the reader is referred to the web version of this article.)

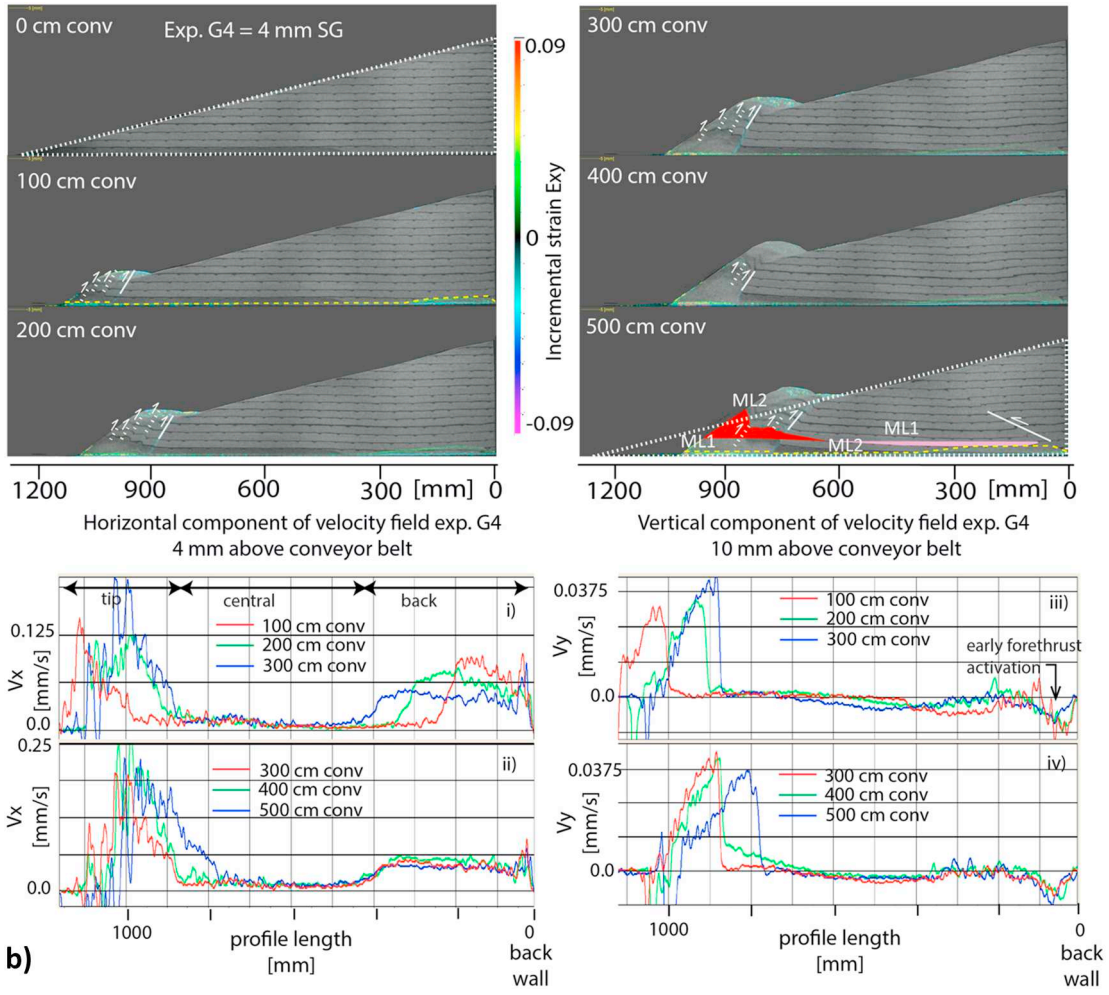

Fig. 7. (*continued*)

backthrusts during further convergence, considerably increasing the area of basal accretion (E in Fig. 6b.v and .vi). Therefore, when G6 is compared to the G4 and G2 experiments, the first indicates that lower surface uplift is caused by lower rates of basal accretion (Figs. 4, 5a and 7). Indeed, the larger basal accretion in experiment G4 in comparison to G2 indicates that the SG parameter was not the only or dominant control on material balance. The more material was removed from the system, the more likely it was to form a localized shear zone. Only in experiments G6 and G4, an active forethrust was occasionally observed. In experiment G4 this forethrust affected mass transfer modes since the early stages of the experiment. This was not evident from the marker lines on the images until a late state of convergence, but could be visualized as downward particle displacement between 50 and 80 mm from the backwall as can be seen in Fig. 7b. As a consequence, the forethrust led to high rates and large amounts of both frontal erosion and basal accretion (Figs. 5 and 10). This observation explains their counter-intuitive larger volumes compared to experiment G2.

4.5. The IC/SG impact on basal erosion

Following the SC concept of Cloos and Shreve (1988a), the IC/SG ratio (TC/SG for our experiments) determines SC behavior and thus wedge evolution. Relations of TC/SG (~2.5, 1.4 and 0.8 mm for G2, G4, and G6 respectively; Table 3) revealed that frontal erosion is linked to the TC/SG ratio. If TC < SG, frontal erosion was controlled by the SG (G6), and if TC > SG, by TC (G2 and G4 wedges). This was depicted

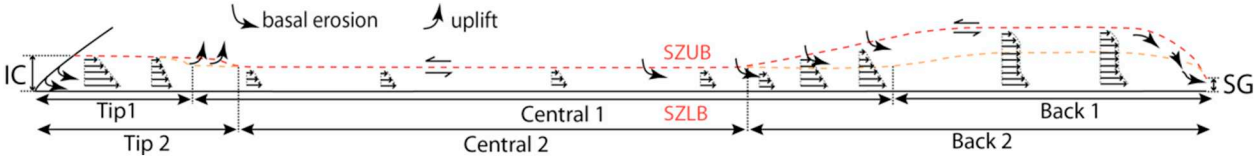

Fig. 8. Sketch of main characteristics of a generic SC, as observed in experiments G4 and G6 (not to scale; in experiment G2 the Back segment would be similar to the Central segment). The SC is confined by upper and lower continuous active shear zones (SZUB and SZLB). Arrows illustrate magnitude and direction of displacement of single particles inside the SC. The lateral differences of the vector velocity field define its Tip, Central and Back segments. The thickness and width of the SC segments were transient over time, here illustrated with Tip1, Central1 and Back1 during a first step of convergence and Tip2, Central2 and Back2 during a second step of convergence (Back1 and 2 segments are absent in experiment G2). The upper boundary of the Back segment additionally underwent an upward migration due to the dynamics of the fastest particles. The transverse velocity gradient behaves as that of a channel flow (the velocity at the bottom is the largest and decreases upward until reaching its lowest value at the top). Basal erosion occurs along the contact with the Central and Back segments but is the strongest where the SC thickens, i.e. the frontal part of the Back segment.

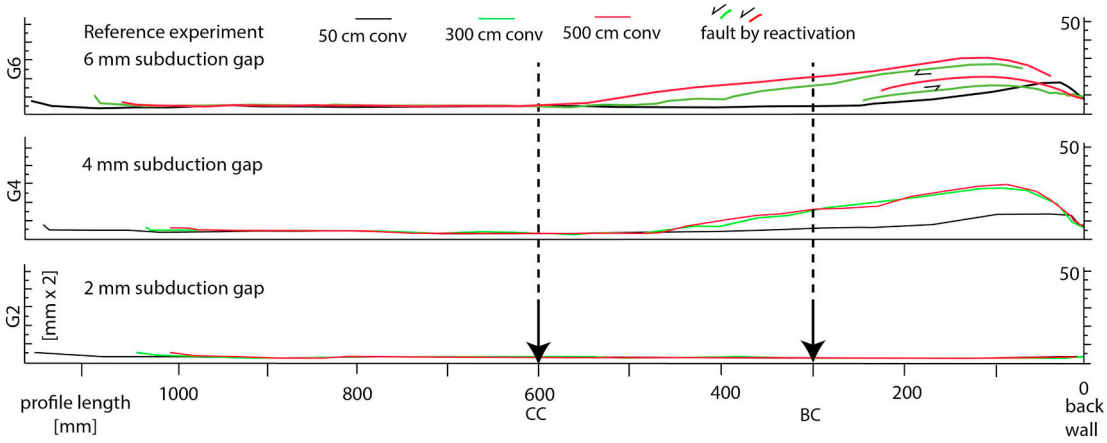

Fig. 9. Subduction channel thickness evolution for the different experiments of the series. CC and BC are (control) points at the Central and Back segments of the SC, corresponding to distances at 600 cm and 300 cm from the backwall, respectively.

with high and similar final volumes of frontal erosion when TC/SG > 1 and a major difference for TC/SG < 1 (70% larger for G2 and 95% larger for G4; Fig. 10). Besides, a ratio TC/SG > 1 was linked to low rates of basal erosion (Table 2). Fig. 5a also shows that, regardless of TC/SG ratio, there may be a direct relation between frontal erosion and tip retreat that additionally controlled the amount of basal accretion. The rates of frontal erosion showed an almost perfectly coeval response to the fluctuations of the basal accretion rates, less evident for tip retreat. Smaller volumes of basal erosion, controlled by the SG size, went together with lower and almost zero subsidence at the middle and upper slopes in the case of G2. Those segments of the SC not affected by the backwall or the toe of the wedge (i.e. point CC in Fig. 9) behaved similar in all experiments resulting in similar fluxes.

Material transfer was largely affected by the SC evolution. Due to the episodic slumps at the front, supply of material to the SC also occurred episodically, and probably provided more material than would be expected from the estimated IC (Table 3). Hence this excess material passing through the SC was accreted at the point where the overburden was large enough to make further transport energetically unfeasible. This restricted the mobility of some of the particles (Tip to Central segments). From this point onwards, particle velocity decreased and remained uniform along the Central segment, therefore decreasing SC thickness.

5. Discussion

Although analogue experiments have highly idealized set-ups, when properly scaled, they offer the possibility to analyze processes in nature. In the following section, we first compare our experiments with those of former analogue, and then discuss possible implications from the experiments to a better understanding of processes that take place at natural convergent margins.

5.1. Comparison with former analogue experiments

Our experiments confirm that subduction erosion (frontal and basal) and basal accretion take place simultaneously, as was first suggested by Kukowski et al. (1994) and then also observed by Lohrmann et al. (2006). The new series of experiments also provides evidence that underplating becomes significant as soon as TC is larger than SG. Hence, sediment underplating resulting from basal accretion may be widespread along the world's convergent margins. As the experimental wedges of Gutscher et al. (1998b) received considerable input of material at the tip, net basal erosion from the backstop only took place when the amount of input material was smaller than the SG times the width of the utilized sandbox. In contrast, in our experiments without incoming sediment and with a subduction gap, the removal of material from the underside of the wedge toe was forced. Normal faulting and subsidence near the lower slope along with tilting was observed in all experiments mentioned so far (in ours, they occurred just before frontal slumps), implying that these processes may all be typical features of natural erosional forearcs.

Lohrmann et al. (2006) related reactivation of the fault along the SZUB to basal erosion (which would refer to where the emergence of the fault or the highest incremental strain occurs; see also Fig. 4iv). The reactivation of fault structures as observed in our wedges as well as in

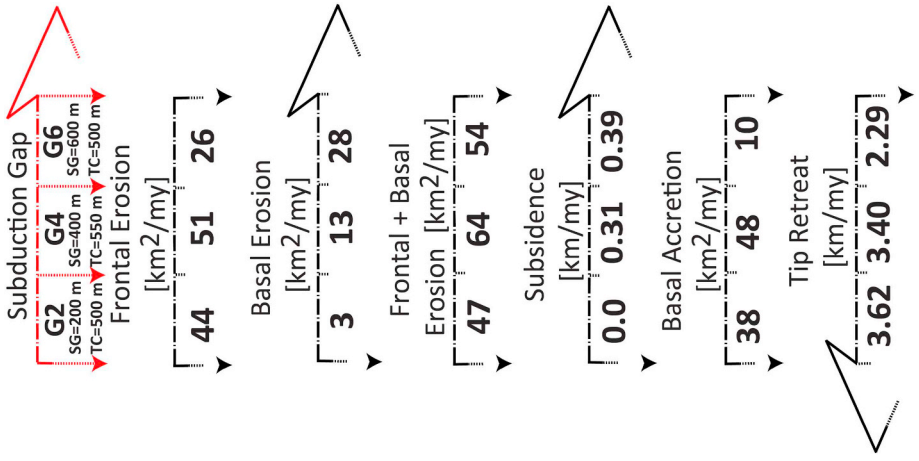

Fig. 10. Bulk mass transfer rates expressed as equivalent values in nature (km eroded/Ma) derived from the final values o the bulk areas/displacement during the second phase (after 50 cm of convergence). Arrow heads show the trend direction of mass transfer increments, where no clear trend is discernible no arrow heads are displayed.

Table 3
Thickness and velocities at specific locations along the profile length during convergence. Thickness and velocities correspond to the average of the different values every 50 cm of convergence during convergence. Numbers between brackets are the standard deviations, which become larger by the seaward migration of the Back segment that ultimately broadens the SC.

	G2 = SG 2 mm	G4 = SG 4 mm	G6 = SG 6 mm
SC thickness at tip segment. = TC [mm]	5	5,5	5
SC thickness at 600 mm = CC [mm]	2,58 (± 0.5)	2,73 (± 0.53)	4,60 (± 0.77)
SC velocity at 600 mm [mm/s]	0,009 (± 0.004)	0,010 (± 0.003)	0,006 (± 0.002)
SC thickness at 300 mm = BC [mm]	2,42 (± 0.54)	6,55 (± 3.3)	11,07 (± 4.9)
SC velocity at 300 mm [mm/s]	0,013 (± 0.003)	0,03 (± 0.013)	0,03 (± 0.012)
Erosional ratio (basal erosion/frontal erosion)	0,07	0,25	1,08
TC/SG	2,5	1,38	0,83
Flux at 600 cm = CC [mm/s]	0,023 (± 0.012)	0,028 (± 0.008)	0,0260 (± 0.009)
Flux at 300 cm = BC [mm/s]	0,03 (± 0.01)	0,207 (± 0.13)	0,3742 (± 0.24)
Estimated IC [mm/cm conv]	4,4	5,1	2,6

those of Lohrmann et al. (2006) may correspond to Riedel shear faults like the ones described by Collot et al. (2011). Apart from facilitating the migration of fluids out of the SC (von Huene et al., 2004), they would accommodate the subsiding rock layer in the new space created by the rotation of the fault. Nevertheless, in experiment G6 at 280 cm of convergence, the reactivated fault locally controlled material flux, such that flux decreased rearward of the reactivated fault (Fig. 6c at 20 cm profile length). However, as subsidence of the middle slope not only took place in experiment G6 but also in experiment G4, in which faults were not reactivated, there must be also other parameter favoring subsidence, e.g. convergence rate, sediment supply to the trench, etc.

5.2. Comparison with nature

Common geometric features recognized in several erosional convergent margins include small frontal prisms (5–20 km wide and ~1–2 km high), large tapers, extensional structures including normal faulting, landward tilted blocks and seaward tilted forearcs (e.g. Aleutians, Scholl et al. (2002); midslope Tonga, Clift and MacLeod (1999); Guatemala, Aubouin et al. (1984); Peru, Bourgois et al. (1988); Chile, von Huene et al. (1999); Mariana Islands, Wessel et al. (1994)), or active mass wasting and related irregular surface slopes (e.g. Japan, Cadet et al., 1987). Such features have also been observed in our experiments, as e.g. the small frontal prism and subsidence in the G6 experiment. Subsidence was also observed along the surface of the Middle segment in experiments G4 and G6, and due to oversteepening, continuous slumping at the Frontal segment occurred.

The geometric features of our experimental wedges mirror what occurs inside the SC. This is in line with the subduction channel concept of Cloos and Shreve (1988a,b) which explains tectonic growth or consumption of the upper plate in forearcs (Beaumont et al., 1999; Ellis et al., 1999; Lohrmann et al., 2006). Subduction erosion is revealed in seismic images (Ranero and von Huene, 2000), and from field studies (Vannucchi et al., 2008). However, since direct observation of the processes within a SC is not possible, we can only speculate about flux mechanics taking place there. As suggested by Cloos and Shreve (1988b), subduction erosion occurs wherever the shear stress is large enough to allow erosion along the SZUB. In our experimental wedges, enhanced basal erosion was occurring closely connected to where the highest shear stress took place (Figs. 4 and 8). Thus, the digital images show evidence that the particle velocity inside the SC is not homogeneously distributed and that different velocity patterns determine the loci of erosion or accretion (Fig. 8), respectively.

The experiments of this study show that even small variations of the subduction gap's size strongly control material transfer through a wedge in an erosive convergent setting. The thickness of the SG controls the thickness of the SC's back segment, which in turn controls fluxes and/or the volume of eroded material. In the experiment with the largest SG, upscaled subsidence rate was about 0.4 km/Ma, which is similar to what has been observed in nature (e.g. Vannucchi et al., 2004). Consequently, in nature a difference of only 200 m in the thickness of the SG might turn an accretionary margin into an erosive one (case for G4 and G6). From this observation, we suggest that whatever process is able to create a subduction window in nature, such as slab rollback (e.g. North of Chile, Manea et al., 2012; Central Mexico, Ferrari et al., 2015; Straub et al., 2015), changes in slab-dip (e.g. North of Chile, Contreras-Reyes et al., 2012; Central Chile and Japan, Lallemand et al., 2005), or large density changes of the upper plate (e.g. Maksymowicz et al., 2015), it may influence the distribution of velocities along the base of the wedge.

At most erosive convergent margins, the forearc slope is segmented into lower, middle and upper slopes (Fig. 1). At the lower slope, the disrupted topography of the frontal prism seems to be due to continuous gravitational collapse, which was observed in the experimental wedges as a consequence of frontal erosion. At the middle-upper slope, sediment and rock ablation from the underside of the forearc have been inferred from typical structures and processes like forearc subsidence, thinning, truncation, extensional structures across the sediment apron and seaward tilting of the surface slope (Fig. 1; Scholl et al., 1980; von Huene and Lallemand, 1990). The forearc block was subject to long-

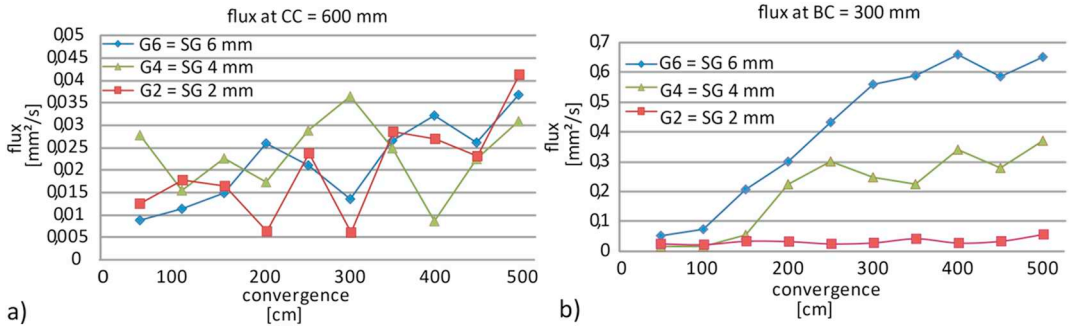

Fig. 11. Fluxes every 50 cm of convergence at a distance a) CC = 600 cm and b) BC = 300 cm from the backwall (for location see Fig. 9).

term subsidence (> 10 Ma) with simultaneous tilting and normal faults deforming either the middle or upper slope, or both (von Huene and Ranero, 2003). At some natural forearcs, numerous faults with a relatively small vertical displacement are outcropping at the forearc surface (< 300 m; Peru and Japan margins), compared to subsidence (4–6 km at the Peru and Japan margins; von Huene and Lallemand, 1990). The transient Back segment of our experimental wedges defined a segmentation of the slope of the wedge, as observed in erosional margins. Nevertheless, the middle and upper slopes in all experiments subsided not by discrete shear zones (as observed in nature), but by distributed deformation. This was attributed to the intrinsic features of granular materials, which differs from that of a consolidated, low porosity cohesive brittle rock. Packing and grain-size distribution of sand cannot be accurately scaled to nature, thus faulting does not occur as discrete failure, but as dilatant shear bands. The localized shear planes are characterized by a local increase in porosity within a tabular band of an average thickness of 1–2 mm (ca. 2–5 grains of sand; Du Bernard et al., 2002).

Rates of subduction erosion seem to fluctuate with time. This has been observed at natural convergent margins like Costa Rica, where periods of slower subduction erosion may alternate with times of faster erosion and trench retreat (mean rate of subsidence of 0.25 km/Ma vs 0.6 km/Ma, respectively; Vannucchi et al., 2003, 2016). Wang et al. (2010) also proposed a cyclic behavior for subduction erosion within seismic cycles. In experiments G4 and G6, velocities of material transfer varied with time, revealing that basal erosion is probably an irregular process and that the thickness of the SG appears to play a role in its fluctuations. However, the timescales on which these temporal fluctuations occur are very different, such that it may well be that subduction erosion processes are transient due to several, so far not well constrained or even unknown processes.

In most aspects, experiment G4 is similar to experiment G6, especially with regard to the rearward portion of the SC, although its SG is thinner. Both experiments also show more similarities with natural erosive convergent margins compared to experiment G2 with a very thin SG. Along the Andean convergent margin, trench fill varies significantly (e.g. Hoffmann-Rothe et al., 2006). Forearc segments showing all features of an erosive margin typically are characterized by a trench fill of only 100 to 300 m, indicating that such a thin sediment layer will not be accreted at the frontal edge of the forearc, but would become part of the SC, while the margin lastly would undergo subduction erosion. The higher similarity of G4 and G6 wedges with natural wedges would be in line with available seismic images that reveal SCs with a thickness of 500 m or more, and thus indicate that upscaling experimental results to nature should be justified.

6. Conclusions

In our analogue experiments on subduction erosion, we observed that wedges with a thin SG developed a SC with uniform velocities along the base of the wedge beyond the Frontal segment. A thick SG led to the development of a SC with an inhomogeneous distribution of velocities along the base of the wedge, segmenting the SC and also the wedge above it. In nature, segmentation of the continental slope with the slope becoming shallower towards the interior of the orogen is indicative of basal removal of material beneath the middle and upper slope, as basal erosion and subsidence depend on the size of the SG.

Basal erosion exceeded frontal erosion when the capacity of the subduction gap was larger than the capacity of the subduction channel close to the tip of the wedge. At a natural convergent margin, this would imply that a relation IC < SG is sufficient to ensure a larger horizontal component of the velocity field at the Back segment than at the Tip segment. A thick SC formed at the rear part of the wedge, when the capacity of the subduction gap was similar or larger than the capacity of the SC close to the tip of the wedge. The segmentation was identified from the distribution of the material flux velocity within the subduction channel. As we observed considerable basal accretion in all experiments, we suggest that underplating of sediment from the subduction channel to the base of the overriding plate may be widespread in nature.

How the material is transported inside the SC continues to be enigmatic, thus more research is needed. However, this first series of sandbox experiments dedicated to the study of subduction erosion and analyzed with a PIV system led to a significant increase of our understanding of processes otherwise very difficult to visualize. The wedges of our sandbox experiments were geometrically consistent with seismic images of natural erosive convergent margins and therefore we are confident to suggest that the geometry of an erosive convergent margin is related to the conditions within the SC.

Acknowledgements

This study was funded by the National Commission for the investigation, science and technology CONICYT (Comisión Nacional de Investigación Científica y Tecnológica) of the Government of Chile, through a scholarship “Beca Presidente de la República” to Francisca Albert. We thank M. Moreno, C. Sippl, L. Pinto, K. Leever, and M. Rosenau for useful support and discussion as well as the two anonymous reviewers for their valuable comments, which significantly improved this manuscript. We also would like to thank T. Ziegenhagen and F. Neumann for technical support in the laboratory.

References

Adam, J., Urai, J., Wieneke, B., Oncken, O., Pfeiffer, K., Kukowski, N., Lohrmann, J., Hoth, S., van der Zee, W., Schmatz, J., 2005. Shear localization and strain distribution during tectonic faulting: new insights from granular-flow experiments and high-resolution optical image correlation techniques. J. Struct. Geol. 27, 283–301. https://doi.org/10.1016/j.jsg.2004.08.008.

Albert, F., 2013. Identification of Kinematic Boundary Conditions Triggering Removal of Material in Tectonically Erosive Margins (PhD Thesis). Freie Universität Berlin – GeoForschungZentrum Potsdam, Berlin-Potsdam, Germany (150 pp.).

Aubouin, J., Bourgois, J., Azema, J., 1984. A new type of active margin: the convergent-extensional margin, as exemplified by the Middle America Trench off Guatemala. Earth Planet. Sci. Lett. 67, 211–218.

Beaumont, C., Ellis, S., Pfiffner, A., 1999. Dynamics of sediment subduction-accretion at convergent margins: short-term modes, long-term deformation, and tectonic implications. J. Geophys. Res. 104 (B8), 17573–17602.

Bonini, M., 2007. Deformation patterns and structural vergence in brittle–ductile thrust wedges: an additional analogue modelling perspective. J. Struct. Geol. 29, 141–158.

Bourgois, J., Pautot, G., Bandy, W., Boinet, T., Chotin, P., Huchon, P., Mercier de Lepinay, B., Monge, F., Monlau, J., Pelletier, B., Sosson, M., von Huene, R., 1988. Sea beam and seismic reflection imaging of the tectonic regime of the Andean continental margin off Peru (4°S to 10°S). Earth Planet. Sci. Lett. 87, 111–126.

Cadet, J.P., Kobayashi, K., Aubouin, J., Boulegue, J., Dubois, J., von Huene, R., Jolivet, L., Kanazawa, T., Kasahara, J., Koizumi, K., Lallemand, S., Nakamura, Y., Pautot, G., Suyehiro, K., Tani, S., Tokuyama, H., Yamazaki, T., 1987. The Japan trench and its juncture with the Kuril trench: cruise results of the KAIKO project, Leg 3. Earth Planet. Sci. Lett. 83, 267–284.

Calahorrano, A., Sallares, V., Collot, J.Y., Sage, F., Ranero, C., 2008. Non linear variations of the physical properties along the southern Ecuador subduction channel: results from depth-migrated seismic data. Earth Planet. Sci. Lett. https://doi.org/10.1016/j.epsl.2007.11.061.

Calassou, S., Larroque, C., Malavieille, J., 1993. Transfer zones of deformation in thrust wedges: an experimental study. Tectonophysics 221, 325–344.

Clift, P.D., MacLeod, C.J., 1999. Slow rates of tectonic erosion estimated from the subsidence and tilting of the Tonga Forearc Basin. Geology 27, 411–414. https://doi.org/10.1130/0091-7613(1999)027<0411:SROSEE>2.3.CO;2.

Clift, P., Vannucchi, P., 2004. Controls on tectonic accretion versus erosion in subduction zones: implications for the origin and recycling of the continental crust. Rev. Geophys. 42, RG4001. https://doi.org/10.1029/2003RG000127.

Clift, P.D., Pecher, I., Kukowski, N., Hampel, A., 2003. Tectonic erosion of the Peruvian forearc, Lima Basin, by subduction and Nazca Ridge collision. Tectonics 22, 1023. https://doi.org/10.1029/2002TC001386.

Cloos, M., Shreve, R.L., 1988a. Subduction-channel model of prism accretion, melange formation, sediment subduction, and subduction erosion at convergent plate margins: 1. Background and description. Pure Appl. Geophys. 128 (3–4), 455–500. https://doi.org/10.1007/BF00874548.

Cloos, M., Shreve, R.L., 1988b. Subduction-channel model of prism accretion, melange formation, sediment subduction, and subduction erosion at convergent plate margins: 2. Implications and discussion. Pure Appl. Geophys. 128 (3–4), 501–545. https://doi.org/10.1007/BF00874549.

Collot, J.Y., Ribodetti, A., Agudelo, W., Sage, F., 2011. The South Ecuador subduction

channel: evidence for a dynamic mega-shear zone from 2D fine-scale seismic reflection imaging and implications for material transfer. J. Geophys. Res. 116, B11102. https://doi.org/10.1029/2011JB008429.
Contreras-Reyes, E., Jara, J., Grevemeyer, I., Ruiz, S., Carrizo, D., 2012. Abrupt change in the dip of the subducting plate beneath north Chile. Nat. Geosci. 5, 342–345.
Dahlen, F.A., 1984. Noncohesive critical Coulomb wedges: an exact solution. J. Geophys. Res. 89, 10125–10133.
Davis, D., Suppe, J., Dahlen, F.A., 1983. Mechanics of fold-and-thrust belts and accretionary wedges. J. Geophys. Res. 88, 1153–1172.
DeMets, C., Dixon, T.H., 1999. New kinematic models for Pacific-North America motion from 3 Ma to present: I. Evidence for steady motion and biases in the NUVEL-1A model. Geophys. Res. Lett. 26, 1921–1924.
Du Bernard, X., Eichhubl, P., Aydin, A., 2002. Dilation bands: a new form of localized failure in granular media. Geophys. Res. Lett. 29 (24), 2176. https://doi.org/10.1029/2002GL015966.
Ellis, S., Beaumont, C., Pfiffner, O.A., 1999. Geodynamic models of crustal-scale episodic tectonic accretion and underplating in subduction zones. J. Geophys. Res. 104 (B7), 15169–15190. https://doi.org/10.1029/1999JB900071.
Ferrari, L., Chiara, M., Francalanci, L., 2015. Generation of oceanic-island basalt–type volcanism in the western Trans-Mexican volcanic belt by slab rollback, asthenosphere infiltration, and variable flux melting. Geology 29, 507–510. https://doi.org/10.1130/0091-7613.
Friederich, W., Lambrecht, L., Stöckhert, B., Wassmann, S., Moos, C., 2014. Seismic visibility of a deep subduction channel – insights from numerical simulation of high-frequency seismic waves emitted from intermediate depth earthquakes. Solid Earth 5, 141–159. https://doi.org/10.5194/se-5-141-2014.
Graveleau, F., Malavieille, J., Dominguez, S., 2012. Experimental modelling of orogenic wedges: a review. Tectonophysics 538–540, 1–66. https://doi.org/10.1016/j.tecto.2012.01.027.
Gutscher, M.A., Kukowski, N., Malavieille, J., Lallemand, S.E., 1996. Cyclical behavior of thrust wedges: insights from high basal friction sandbox experiments. Geology 24, 135–138.
Gutscher, M.A., Kukowski, N., Malavieille, J., Lallemand, S.E., 1998a. Episodic imbricate thrusting and underthrusting: analog experiments and mechanical analysis applied to the Alaskan Accretionary Wedge. J. Geophys. Res. 103, 10161–10176. https://doi.org/10.1029/97JB03541.
Gutscher, M.A., Kukowski, N., Malavieille, J., Lallemand, S.E., 1998b. Material transfer in accretionary wedges from analysis of a systematic series of analog experiments. J. Struct. Geol. 20, 407–416.
Hampel, A., Adam, J., Kukowski, N., 2004. Response of the tectonically erosive South Peruvian forearc to subduction of the Nazca ridge: analysis of 3D analogue experiments. Tectonics 23, TC5003. https://doi.org/10.1029/2003TC001585.
Heki, K., 2004. Space geodetic observation of deep basal subduction erosion in northeastern Japan. Earth Planet. Sci. Lett. 219, 13–20.
Hoffmann-Rothe, A., Kukowski, N., Dresen, G., Echtler, H., Oncken, O., Klotz, J., Scheuber, E., Kellner, A., 2006. Oblique convergence along the Chilean margin: Partitioning, margin-parallel faulting and force interaction at the plate interface. In: Oncken, O. (Ed.), Andean Geodynamics, Frontiers Geosci. vol. 1 Springer, New York (in press).
Hubbert, M.K., 1937. Theory of scale models as applied to the study of geological structures. Bull. Geol. Soc. Am. 48, 1459–1520.
Keppie, D.F., Currie, C., Warren, C., 2009. Subduction erosion modes: comparing finite element numerical models with the geological record. Earth Planet. Sci. Lett. https://doi.org/10.1016/j.epsl.2009.08.009.
Konstantinovskaja, E., Malavieille, J., 2005. Erosion and exhumation in accretionary orogens: experimental and geological approaches. Geochem. Geophys. Geosyst. 6 (2), 1–24. https://doi.org/10.1029/2004GC000794.
Kopp, H., Kukowski, N., 2003. Backstop geometry and accretionary mechanics of the Sunda margin. Tectonics 22 (6), 1072. https://doi.org/10.1029/2002TC001420. (1–16).
Koyi, H.A., 1997. Analogue modelling; from a qualitative to a quantitative technique, a historical outline. J. Pet. Geol. 20, 223–238. https://doi.org/10.1111/j.1747-5457.1997.tb00774.x.
Kukowski, N., Onken, O., 2006. Subduction erosion – the “normal” mode of fore-arc material transfer along the Chilean margin? In: Oncken, O., Chong, G., Franz, G., Giese, P., Götze, H.-J., Ramos, V.A., Strecker, M.R., Wigger, P. (Eds.), The Andes – Active Subduction Orogeny. Frontiers in Earth Science Series, vol. 1. Springer-Verlag, Berlin Heidelberg New York, pp. 216–236.
Kukowski, N., von Huene, R., Malavieille, J., Lallemand, S., 1994. Sediment accretion against a buttress beneath the Peruvian continental margin as simulated by sandbox modeling. Geol. Rundsch. 83, 822–831.
Kukowski, N., Malavieille, J., Gutscher, M.A., Lallemand, S.E., Reston, T.J., 2002. Mechanical decoupling and basal duplex formation observed in sandbox experiments with application to the Western Mediterranean Ridge accretionary complex. Mar. Geol. 187, 29–42.
Lallemand, S.E., Schnurle, P., Manoussis, S., 1992a. Reconstruction of subduction zone paleogeometries and quantification of upper plate material losses caused by tectonic erosion. J. Geophys. Res. 97, 217–239. https://doi.org/10.1029/91JB02342.
Lallemand, S.E., Malavieille, J., Calassou, S., 1992b. Effects of oceanic ridge subduction on accretionary wedges: experimental modeling and marine observations. Tectonics 11, 1301–1313. https://doi.org/10.1029/92TC00637.
Lallemand, S.E., Schnurle, P., Malavieille, J., 1994. Coulomb theory applied to accretionary and non-accretionary wedges: possible causes for tectonic erosion and/or frontal accretion. J. Geophys. Res. 99, 12033–12055. https://doi.org/10.1029/94JB00124.
Lallemand, S., Heuret, A., Boutelier, D., 2005. On the relationships between slab dip, back-arc stress, upper plate absolute motion, and crustal nature in subduction zones. Geochem. Geophys. Geosyst. 6, Q09006. https://doi.org/10.1029/2005GC000917.
Lohrmann, J., Kukowski, N., Adam, J., Oncken, O., 2003. The impact of analogue material parameters on the geometry, kinematics, and dynamics of convergent sand wedges. J. Struct. Geol. 25, 1691–1711. https://doi.org/10.1016/S0191-8141(03)00005-1.
Lohrmann, J., Kukowski, N., Krawczyk, C.M., Oncken, O., Sick, C., Sobiesiak, M., Rietbrock, A., 2006. Subduction channel evolution in brittle forearc wedges – a combined study with scaled sandbox experiments, seismological and reflection seismic data and geological field evidence. In: Oncken, O., Chong, G., Franz, G., Giese, P., Götze, H.J., Ramos, V.A., Strecker, M.R., Wigger, P. (Eds.), The Andes – Active Subduction Orogeny. Frontiers in Earth Science Series, vol. 1. Springer-Verlag, Berlin Heidelberg New York, pp. 237–262.
Maksymowicz, A., Tréhu, A., Contreras-Reyes, E., Ruiz, S., 2015. Density-depth model of the continental wedge at the maximum slip segment of the Maule Mw8.8 megathrust earthquake. Earth Planet. Sci. Lett. 409, 265–277.
Manea, V.C., Pérez-Gussinyé, M., Manea, M., 2012. Chilean flat slab subduction controlled by overriding plate thickness and trench rollback. Geology 40, 35–38.
McClay, K.R., 1996. Recent advances in analogue modelling: uses in section interpretation and validation. In: Buchanan, P.G., Nieuwland, D.A. (Eds.), Modern Developments in Structural Interpretation, Validation and Modelling. Geological Society Special Publication, vol. 99. pp. 201–225.
Miller, H., 1970. Das Problem des hypothetischen Pazifischen Kontinentes gesehen von der chilenischen Pazifikküste. Geol. Rundsch. 59, 927–938.
Nilforoushan, F., Koyi, H., Swantesson, J.O.H., Talbot, C., 2008. Effect of basal friction on surface and volumetric strain in models of convergent settings measured by laser scanner. J. Struct. Geol. 30, 366–379. https://doi.org/10.1016/j.jsg.2007.09.013.
Oncken, O., 1998. Evidence for precollisional subduction erosion in ancient collisional belts: the case of the Mid-European Variscides. Geology 26 (12), 1075–1078. https://doi.org/10.1130/0091-7613(1998)026<1075:EFPSEI>2.3.CO;2.
Patzig, R., Shapiro, S., Asch, G., Giese, P., Wigger, P., 2002. Seismogenic plane of the northern Andean subduction zone from aftershocks of the Antofagasta (Chile) 1995 earthquakes. Geophys. Res. Lett. 29, 1264. https://doi.org/10.1029/2001GL013244.
Ranero, C.R., von Huene, R., 2000. Subduction erosion along the Middle America convergent margin. Nature 404 (6779), 748–752.
Ranero, C.R., Grevemeyer, I., Sahling, H., Barckhausen, U., Hensen, C., Wallmann, K., Weinrebe, W., Vannucchi, P., von Huene, R., McIntosh, K., 2008. The hydrogeological system of erosional convergent margins and its influence on tectonics and interplate seismogenesis. Geochem. Geophys. Geosyst. 9 (3), Q03S04. https://doi.org/10.1029/2007GC001679.
Rutland, R.W.R., 1971. Andean orogeny and ocean floor spreading. Nature 233, 252–255.
Sage, F., Collot, J.Y., Ranero, C., 2006. Interplate patchiness and subduction-erosion mechanisms: evidence from depth migrated seismic images at the Central Ecuador convergent margin. Geology 34 (12), 997–1000. https://doi.org/10.1130/G42790A.1.
Schellart, W.P., 2000. Shear test results for cohesion and friction coefficients for different granular materials: scaling implications for their usage in analogue modeling. Tectonophysics 324, 1–16.
Scholl, D.W., von Huene, R., Vallier, T.L., Howell, D.G., 1980. Sedimentary masses and concepts about tectonic processes at underthrust ocean margins. Geology 8, 564–568.
Scholl, D.W., von Huene, R., Ryan, H.F., 2002. Basal subduction erosion and the formation of the Aleutian Terrace and underlying forearc basin. In: Program and Abstracts, 3rd Biennial Workshop on Subduction Processes Emphasizing the Kurile-Kamchatka-Aleutian Arc. Geophys. Inst., Univ. of Alaska, Fairbanks, pp. 61–62.
Schulze, D., 2007. Powders and Bulk Solids: Behavior, Characterization, Storage and Flow. Springer (511 pp.).
Shreve, R., Cloos, M., 1986. Dynamics of sediment subduction, Melange Formation, and prism accretion. J. Geophys. Res. 911, 10229–10245. https://doi.org/10.1029/JB091iB10p10229.
Stern, C.R., 2011. Subduction erosion: rates, mechanisms, and its role in arc magmatism and the evolution of the continental crust and mantle. Gondwana Res. 20, 284–306. https://doi.org/10.1016/j.gr.2011.02.006.
Straub, S., Gómez-Tuena, A., Bindeman, I., Bolge, L., Brandl, P., Espinasa-Perena, R., Solari, L., Stuart, F., Vannucchi, P., Zellmer, G., 2015. Crustal recycling by subduction erosion in the central Mexican Volcanic Belt. Geochim. Cosmochim. Acta 166, 29–52. https://doi.org/10.1016/j.gca.2015.06.001.
Tsuru, T., Park, J.O., Takahashi, N., Kodaira, S., Kido, Y., Kaneda, Y., Kono, T., 2000. Tectonic features of the Japan Trench convergent margin and fracture zones beneath northeastern Japan revealed by multi-channel seismic reflection data. J. Geophys. Res. 105, 16403–16413. https://doi.org/10.1029/2000JB900132.
Vanneste, L., Larter, R., 2002. Sediment subduction, subduction erosion, and strain regime in the northern South Sandwich forearc. J. Geophys. Res. 107 (B7), 2149. https://doi.org/10.1029/2001JB000396.
Vannucchi, P., Ranero, C.R., Galeotti, S., Straub, S.M., Scholl, D.W., McDougall-Ried, K., 2003. Fast rates of subduction erosion along the Costa Rica Pacific margin: implications for nonsteady rates of crustal recycling at subduction zones. J. Geophys. Res. 108 (B11), 2511. https://doi.org/10.1029/2002JB002207.
Vannucchi, P., Galeotti, S., Clift, P., von Huene, C., 2004. Long-term subduction-erosion along Guatemala margin of the Middle America trench. Geology 32 (7), 617–620. https://doi.org/10.1130/G20422.1.
Vannucchi, P., Remitti, F., Bettelli, G., 2008. Geological record of fluid flow and seismogenesis along an erosive subducting plate boundary. Nature 451, 699–703. https://doi.org/10.1038/nature06486.
Vannucchi, P., Morgana, J., Balestrieri, M., 2016. Subduction erosion, and the de-construction of continental crust: the Central America case and its global implications. Gondwana Res. 40, 184–198. https://doi.org/10.1016/j.gr.2016.10.001.

von Huene, R., Lallemand, S., 1990. Tectonic erosion along the Japan and Peru convergent margins. Geol. Soc. Am. Bull. 102, 704–720.
von Huene, R., Ranero, C.R., 2003. Subduction erosion and basal friction along the sediment-starved convergent margin off Antofagasta, Chile. J. Geophys. Res. 108, 2079. https://doi.org/10.1029/2001JB001569.
von Huene, R., Scholl, D., 1991. Observations at convergent margins concerning sediment subduction, subduction erosion, and the growth of continental crust. Rev. Geophys. 29, 279–316. https://doi.org/10.1029/91RG00969.
von Huene, R., Klaeschen, D., Cropp, B., Miller, J., 1994. Tectonic structure across the accretionary and erosional parts of the Japan Trench margin. J. Geophys. Res. 99, 22349–22361. https://doi.org/10.1029/94JB01198.
von Huene, R., Weinrebe, W., Heeren, F., 1999. Subduction erosion along the North Chile margin. J. Geodyn. 27, 345–358.
von Huene, R., Ranero, C.R., Vannucchi, P., 2004. Generic model of subduction erosion. Geology 32, 913–916. https://doi.org/10.1130/G40563.1.
Wang, K., Hu, Y., von Huene, R., Kukowski, N., 2010. Interplate earthquakes as a driver of shallow subduction erosion. Geology 38, 431–434. https://doi.org/10.1130/G30597.1.
Wessel, J., Fryer, P., Wessel, P., Taylor, B., 1994. Extension in the northern Mariana forearc. J. Geophys. Res. 99 (B8), 15181–15203.
White, D.J., Take, W.A., Bolton, M.D., 2001. Measuring soil deformation in geotechnical models using digital images and PIV analysis. In: 10th International Conference on Computer Methods and Advances in Geomechanics. Tucson, Arizona. Balkema, Rotterdam, pp. 997–1002.